PCCP

Accepted Manuscript

ROYAL SOCIETY OF CHEMISTRY

www.rsc.org/pccp

Cite this: DOI: 10.1039/c0xx00000x

www.rsc.org/xxxxxx

ARTICLE TYPE

An ab initio MO study of heavy atom effects on the zero-field splitting tensors of high-spin nitrenes: How the spin–orbit contributions affected

Kenji Sugisaki,[a] Kazuo Toyota,*[a] Kazunobu Sato,*[a] Daisuke Shiomi,[a] Masahiro Kitagawa[b] and Takeji Takui*[a]

Received (in XXX, XXX) Xth XXXXXXXXX 20XX, Accepted Xth XXXXXXXXX 20XX
DOI: 10.1039/b000000x

The CASSCF and the hybrid CASSCF/MRMP2 methods are applied to the calculations of spin–spin and spin–orbit contributions to the zero-field splitting tensors (**D** tensors) of halogen-substituted spin-septet 2,4,6-trinitrenopyridines, focusing on the heavy atom effects on the spin–orbit term of the **D** tensors ($\mathbf{D}^{SO}$ tensors). The calculations reproduced experimentally determined $|D|$ values within an error of 15%. Halogen substitutions at the 3,5-positions are less influential in the spin–spin dipolar ($\mathbf{D}^{SS}$) term of 2,4,6-trinitrenopyridines, although the $\mathbf{D}^{SO}$ terms are strongly affected by the introduction of heavier halogens. The absolute sign of the D^{SO} value ($D = D_{ZZ} - (D_{XX} + D_{YY})/2$) of 3,5-dibromo derivative **3** is predicted to be negative, which contradicts the Pederson–Khanna (PK) DFT result previously reported. The large negative contributions to the D^{SO} value of **3** arise from the excited spin-septet states ascribed mainly to the excitations of in-plane lone pair of bromine atoms → SOMO of π nature. Importance of the excited states involving electron transitions from the lone pair orbital of halogen atom is also confirmed in the $\mathbf{D}^{SO}$ tensors of halogen-substituted *para*-phenylnitrenes. A new scheme based on the orbital region partitioning is proposed for the analysis of the $\mathbf{D}^{SO}$ tensors as calculated by means of the PK-DFT approach.

1. Introduction

In molecules having a spin quantum number $S = 1$ or higher, the degeneracy of the electron spin sublevels can be lifted in the absence of an external magnetic field, which is known as zero-field splitting (ZFS). Experimental and theoretical characterizations of ZFS are important for the understanding of electronic structures of open shell entities such as spin multiplet systems, because ZFS originates in anisotropic nature of magnetic interactions between unpaired electrons. Electron spin resonance (ESR) spectroscopy is widely used for the detection and physico-chemical identification of ZFS, which is characterized by a second rank traceless tensor **D**. Recent rapid progresses in experimental techniques such as matrix isolation technique,[1,2] pulse-ESR based electron spin transient nutation spectroscopy for the discrimination of chemical species of different spin multiplicities,[3–13] and a hybrid eigenfield method for calculating exact resonance fields and transition probabilities[14–17] have enabled us to accurately determine **D** tensors. By contrast, quantitative first principle calculations of **D** tensors have been a long-standing issue in theoretical chemistry and high-spin chemistry.[18] In a perturbation expansion starting from a non-relativistic Schrödinger equation, the spin–spin dipolar (SS) and spin–orbit (SO) couplings appear as the first- and second-order terms, respectively.[18,19] The last decades have witnessed development of quantum chemical computational methods for **D** tensors on the basis of density functional theory (DFT)[20–51] and ab initio[27–30,52–69] methods. The DFT-based approaches for the SS and SO terms of **D** tensors ($\mathbf{D}^{SS}$ and $\mathbf{D}^{SO}$ tensors, respectively) have attracted attention owing to their relatively low computational costs and the availability of published quantum chemistry program packages,[70,71] although some intrinsic difficulties in the DFT-based approaches have been pointed out by several groups[23–31] and sophisticated ab initio methods usually give more reliable results than DFT.

For the ab initio methods, the multiconfigurational self-consistent field (MCSCF)-based approaches have widely been used for the calculations of both the $\mathbf{D}^{SS}$ and $\mathbf{D}^{SO}$ tensors. For the $\mathbf{D}^{SO}$ tensor calculations, a sum-over-states (SOS) equation is frequently used in conjunction with the complete active space self-consistent field (CASSCF) wavefunctions.[52–59] However, the $\mathbf{D}^{SO}$ tensor calculated by means of the SOS-CASSCF method is in some cases far from the experimental one due to inaccurate CASSCF excitation energies. A simple solution to circumvent this difficulty is to take account of dynamical electron correlation effects in the calculation of zeroth order energies by using multireference perturbation theory (MRPT) or multireference configuration interaction (MRCI).[35–37,62–64] We have recently proposed a hybrid CASSCF/multireference second order Møller–Plesset (MRMP2[72–74]) approach[27] for the $\mathbf{D}^{SO}$ tensor calculations. The hybrid CASSCF/MRMP2 method can take into account both nondynamical and dynamical electron correlation effects efficiently, and the method has been one of the most reliable techniques for the calculations of the $\mathbf{D}^{SO}$ tensors of organic spin multiplets, as demonstrated in the nπ* excited triplet states of

diazabenzenes and CS_2,[27] high-spin oligonitrenes and oligocarbenes,[28] and spin-triplet arylnitrenes.[29]

As well known, the introduction of heavy atoms at appropriate positions can strengthen SOC. Essentially SOC plays a role of the universal symmetry breaker and thus gives rise to the mixing of electronic eigenstates which would otherwise orthogonal. Theoretical investigations of the heavy atom effects on the **D** tensors are important not only for materials designs/molecular optimization for novel molecular functionality and but also for a deep insights into the heavy atom effects, which gives a testing ground for the theoretical framework for the **D** tensor calculations. Very recently, stable molecules having large D values ($D = (D_{ZZ} - (D_{XX} + D_{YY})/2$, where D_{XX}, D_{YY}, and D_{ZZ} are the principal values of the **D** tensor) in their electronic ground state have attracted special attention as a candidate for quantum spin memory devices which couple with superconducting flux quantum bits (qubits) at very low temperature.[75] Nitrene compounds (R–N:) have very large D values among organic spin multiplet systems[76] due to short electron spin–spin distances and dominant one–centre interactions. In spite of the fact that nitrenes are typical reaction intermediates, some ground-state triplet or spin-multiplet nitrenes are extremely stable in diamagnetic lattices.[77,78] Quantum chemistry based molecular optimization is crucial in quest for chemical entities with sizable values of ZFS.

In 2012, Misochko and co-workers reported that 3,5-dibromo-substituted spin-quintet 2,6- and 2,4-dinitrenopyridines (**7-Br** and **8-Br**, respectively) and spin-septet 2,4,6-trinitrenopyridine (**3**) generated by the photolysis of the corresponding triazide precursor **4-Br** (see Scheme 1) have significantly large $|D|$ values compared with analogous trinitrenopyridine compounds.[79–82] On the basis of DFT calculations, they concluded that SOC dominantly contributes to the **D** tensors of the dibromo derivatives.[82] However, physical origins of the heavy atom effects have not been identified nor discussed. In this paper, we report the CASSCF and the hybrid CASSCF/MRMP2 calculations of the **D** tensors of halogen-substituted spin-septet 2,4,6-trinitrenopyridines (**1**–**3**), focusing on the heavy atom effects on their **D** tensors in an elaborate manner and discussing significant difference between the present and DFT approaches. We also propose a new scheme based on the orbital region partitioning to analyze the $\mathbf{D}^{SO}$ tensors as calculated by means of the PK-DFT approach.

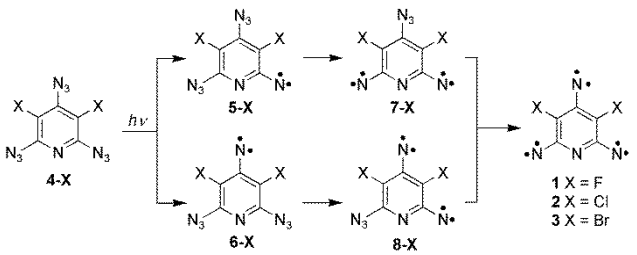

Scheme 1

2. Computational Methods

Equilibrium geometries of **1**–**3** were optimized at the UHCTH/407/6-31G* level of theory using a Gaussian 03 software.[83] No imaginary vibration frequency was obtained at the optimized geometry. The Cartesian coordinates of the optimized geometries are given in ESI.† Molecules **1**–**3** belong to a C_{2v} point group with planar structures.

The $\mathbf{D}^{SS}$ tensor calculations were carried out at the CASSCF(20e,16o)/cc-pVDZ level with a Dalton2011 program package.[84] The CASSCF active space consists of six SOMOs, six valence π and π* orbitals of a pyridine ring, and in-plane and out-of-plane lone pair orbitals of valence p nature of halogen atoms, as illustrated in Fig. 1 for **3**.

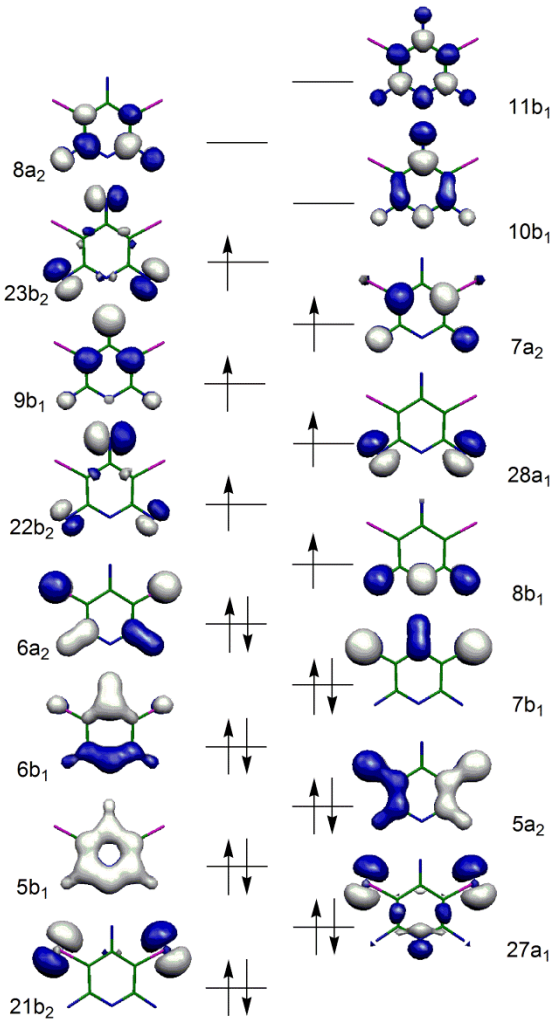

Fig. 1 CASSCF active space and the orbital occupancies in the main configuration of the $1\ ^7A_2$ ground state of **3**.

The $\mathbf{D}^{SO}$ tensors were calculated at the hybrid CASSCF/MRMP2 method. The hybrid CASSCF/MRMP2 approach is based on the sum-over-state equation (eqns (1)–(3)).[27–29,85] In eqn (1), the SOC integrals are evaluated by using the CASSCF wavefunctions, and the excitation energies are computed at the MRMP2 method.

$$D_{ij}^{SO} = \sum_{n,\sigma} C(\sigma) \frac{\left\langle \Psi_{0,S,M}^{\mathrm{CASSCF}} \middle| H_i^{SO} \middle| \Psi_{n,S+\sigma,M}^{\mathrm{CASSCF}} \right\rangle \left\langle \Psi_{n,S+\sigma,M}^{\mathrm{CASSCF}} \middle| H_j^{SO} \middle| \Psi_{0,S,M}^{\mathrm{CASSCF}} \right\rangle}{E_n^{\mathrm{MRMP2}} - E_0^{\mathrm{MRMP2}}} \quad (1)$$

$$C(\sigma=+1)=\frac{1}{2S+1}\ ,\ C(\sigma=0)=-\frac{1}{S^2}\ ,\ C(\sigma=-1)=\frac{1}{2S-1} \quad (2)$$

$$H^{SO}=\frac{\alpha^2}{2}\left\{\sum_{p,A}\frac{Z_A}{r_{pA}^3}\mathbf{l}_A(p)\cdot\mathbf{s}(p) - \sum_{p,q}\frac{1}{r_{pq}^3}\mathbf{l}(p,q)\cdot(\mathbf{s}(p)+2\mathbf{s}(q))\right\} \quad (3)$$

In the $\mathbf{D}^{SO}$ tensor calculations, we used the (20e,16o) active space and cc-pVDZ basis set for CASSCF, the same conditions as in the $\mathbf{D}^{SS}$ tensor calculations. In this study, ten excited states for each irreducible representation of spin-quintet ($\sigma = -1$), septet ($\sigma = 0$), and nonet ($\sigma = +1$) states (totally 90 excited states) were taken into account in the sum-over-states procedure. The full Breit–Pauli spin–orbit Hamiltonian (eqn (3)) that contains spin–same-orbit and spin–other-orbit terms in addition to one electron spin–orbit operator were used for the evaluation of SOC integrals. In the MRMP2 computations, an energy denominator shift technique[86,87] was adopted with a shift parameter $\Delta = 0.02$ Hartree, to avoid divergence of the perturbation energy in the presence of intruder states. These calculations were carried out by using a GAMESS-US program suite.[88]

3. Results and Discussions

ZFS parameters of halogen-substituted 2,4,6-trinitrenopyridines 1–3.

The calculated and experimental ZFS parameters D and E ($E = (D_{XX} - D_{YY})/2$) of **1**–**3** are summarized in Table 1. We choose the D_{ZZ} axis in a conventional manner, to satisfy the relationship of $|E/D| \leq 1/3$. Note that in **2** and **3** the D_{ZZ} axis of $\mathbf{D}^{SO}$ does not coincide with that of $\mathbf{D}^{SS}$ (see Table 2 and Fig. 2 for details), and this is the reason why the D^{SS+SO} value is not a simple scalar sum of D^{SS} and D^{SO} values in **2** and **3**. The $D^{SS}{}_{ZZ}$ axis is perpendicular to the molecular plane in **1**–**3**, but the direction of the $D^{SO}{}_{ZZ}$ axis changes depending on the kind of the substituted halogens. The theoretical D^{SS+SO} values reproduce the experimental $|D|$'s within an error of 15%. In **1** and **2**, the $\mathbf{D}^{SS}$ term has the leading contribution, but the $\mathbf{D}^{SO}$ term becomes prominent in **3**. The absolute sign of the D^{SO} value of **3** is predicted to be negative, which contradicts the reported DFT (PK-PBE/Ahlrichs-DZ) result.[73] We have carried out DFT-based $\mathbf{D}^{SO}$ tensor calculations using Pederson–Khanna (PK),[20] coupled-perturbed (CP),[21] and quasi-restricted orbital (QRO)[22] methods with several pure exchange–correlation functionals (LDA, BP86, BLYP, PBE, RevPBE, and TPSS) and basis sets (Ahlrichs-DZ, cc-pVDZ, and cc-pVTZ) by utilizing ORCA quantum chemistry software,[70] but all the DFT calculations failed to reproduce our hybrid CASSCF/MRMP2 result of **3** even qualitatively (see ESI† for details). We obtained large positive D^{SO} values in **3** by the DFT calculations when the cc-pVDZ and cc-pVTZ basis sets were employed. Only the combination of the CP method and Ahlrichs-DZ basis set gives a negative D^{SO} value in **3**, but the $D^{SO}{}_{ZZ}$ axis is perpendicular to the molecular plane, which contradicts the hybrid CASSCF/MRMP2 result.

The principal values of the $\mathbf{D}^{SS}$ and the $\mathbf{D}^{SO}$ tensors in the coordinate system fixed to the molecular axis are summarized in Table 2. Here, the trinitrene molecules are on the *yz*-plane and the *z*-axis is parallel to the C_2 symmetry axis. The $\mathbf{D}^{SS}$ tensor is hardly perturbed by the introduction of halogen atoms. In the $\mathbf{D}^{SO}$ tensor of **1**, the excited quintet states have the leading contributions with positive signs, and the D^{SO} value is similar to that of 2,4,6-trinitrenotoluene and 2,4,6-trinitrenotriazine.[28] As discussed below, the excited states attributed to (SOMO → SOMO) spin flip electron transitions dominantly contribute to the $\mathbf{D}^{SO}$ tensor of **1**. By the introduction of heavier halogen atoms, the negative $\mathbf{D}^{SO}$ contributions from excited septet states grow rapidly, particularly in the D_{yy} component. The spin quantum number-dependent coefficient $C(\sigma)$ is responsible for the negative sign of the principal values of $\mathbf{D}^{SO}{}_{septet}$. In **2**, the $\mathbf{D}^{SO}$ contributions from excited quintet and septet states are comparable in magnitude with different signs, which results in the reduction of the $\mathbf{D}^{SO}$ contributions. In **3**, the excited septet states become more important with respect to the $\mathbf{D}^{SO}$ contributions, and excited nonet states have non-negligible contributions to the $\mathbf{D}^{SO}$ tensor. Because the $\mathbf{D}^{SO}$ contributions from excited septet and nonet states are highly asymmetric, which reflects the character of the excited states as discussed below, the direction of the $D^{SO}{}_{ZZ}$ axis changes by the halogen substitutions.

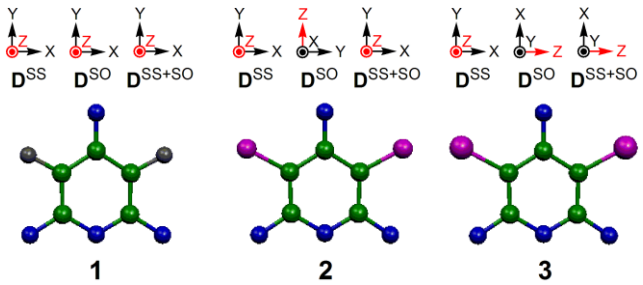

Fig. 2 Principal axes of the $\mathbf{D}^{SS}$, $\mathbf{D}^{SO}$ and $\mathbf{D}^{SS+SO}$ tensors in trinitrenes **1**–**3**.

The important electronic excited states of **1**–**3** with respect to the $\mathbf{D}^{SO}$ tensors are summarized in Tables 3–5, respectively. In all molecules under study, the excited quintet states described mainly by (in-plane SOMO → out-of-plane SOMO) and (out-of-plane SOMO → in-plane SOMO) spin flip excitations contribute positively to the $\mathbf{D}^{SO}$ principal values, which is a tendency similar to typical high-spin arylnitrenes.[28,29] In trinitrene compounds under study, three nitrene sites possess a pseudo-C_3 symmetry, and therefore the $\mathbf{D}^{SO}$ contributions from the (SOMO → SOMO) spin flip excited quintet states are nearly axial symmetric ($D_{yy} \approx D_{zz}$) in **1** and **2**. In **3**, the modulation effects on the spin density distribution caused by the halogen substituents are much stronger than in **1** and **2**, which induces large anisotropy in the $\mathbf{D}^{SO}$ contributions from the (SOMO → SOMO) excited quintet states.

By introducing heavier halogen atoms, the excited states involving electron transitions from the lone pair orbitals of the halogen atoms become more and more important. No wonder that both excitation energies and spin–orbit coupling constants (SOCCs) of these states strongly depend on the kind of substituted halogens. The excited septet states of (lone pair → SOMO) characters are particularly important. In **1**, the spin-septet excited states of (lone pair → SOMO) characters did not appear

within the lowest ten states of the CASSCF solution in each irreducible representation. Namely, the excitation energies of the (lone pair → SOMO) excited septet states are sufficiently high in **1**, leading to negligible $\mathbf{D}^{SO}$ contributions from these excited states (see Fig. 3). Contrastingly, in **2**, the $\mathbf{D}^{SO}$ contributions from the (lone pair → SOMO) excited septet states are comparable in magnitude to those from the excited quintet states. In **3**, the (lone pair → SOMO) excited septet states prominently contribute to the $\mathbf{D}^{SO}$ tensor. Large $\mathbf{D}^{SO}$ contributions clearly arise from both the small excitation energies and the large SOCCs due to the destabilization of the lone pair orbitals and increase of a nuclear charge in heavier halogens. The ratio of the excited septet and quintet (lone pair → SOMO) contributions to D^{SO}_{yy} to those of D^{SO}_{zz} is approximately 5:1 in both **2** and **3**. This remarkable difference in the contributions between the former **1** and the latter **2** and **3** is depicted in the energy diagram of Fig. 3. This large anisotropic character is explained by the orientation of the lone pair orbitals and a symmetry rule of SOC. From the symmetry rule of SOC, electron transitions from the *z*-directed orbitals to the *x*-directed orbitals contribute to the *y*-component of the SOC integrals. In the trinitrene molecules under study, the in-plane lone pair orbitals of valence p nature of the halogen atoms are canted about 30 and −30 degrees from the *z*-axis in the *yz*-plane. The π orbitals are parallel to the *x*-axis. Therefore, the excitations from the lone pair orbitals to the π orbital dominantly contribute to the D_{yy} component with minor contributions to the D_{zz} component.

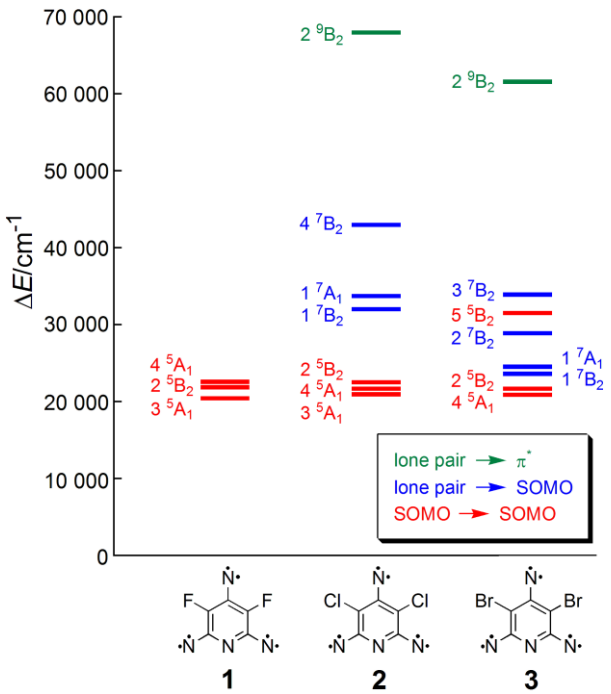

Fig. 3 Energy diagram of the selected excited states with the important SOC contributing weights for **1**–**3**.

In the dibromo derivative **3**, the $\mathbf{D}^{SO}$ contributions from the excited nonet states are too large to neglect. Relatively large $\mathbf{D}^{SO}$ contributions from the excited nonet states are attributed to the (lone pair → π*) excitations such as the 2 $^9B_2$ state. These (lone pair → π*) excited states have high excitation energies, but their SOCCs are large enough to have significant contributions to the $\mathbf{D}^{SO}$ tensor.

ZFS parameters of halogen-substituted *para*-phenylnitrenes 9–12.

To disclose heavy atom effects on the $\mathbf{D}^{SO}$ tensors of halogen-substituted high-spin nitrenes in more detail, the **D** tensor calculations of halogen-substituted *p*-phenylnitrenes **9**–**12** as shown in Scheme 2 were also carried out. In these molecules, the $|D|$ value decreased by the introduction of heavier halogen atoms, and this tendency was explained in terms of the spin polarization and the spin density delocalization mechanisms.[89] It is interesting to investigate the effects of the magnitude of SOC on the decline in the experimental $|D|$ values. In the present calculations, Sapporo-DZP-2012 basis set[90] was used for the geometry optimizations and the CASSCF computations, because cc-pVDZ basis set does not support iodine atom. The CASSCF active space was set to (12e,10o), as illustrated in Fig. 4 for **12**. The results are summarized in Table 6. Note that *E* values of these molecules were determined to be small (< 0.002 cm^{-1}) in the experiment.

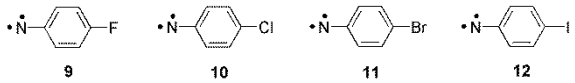

Scheme 2

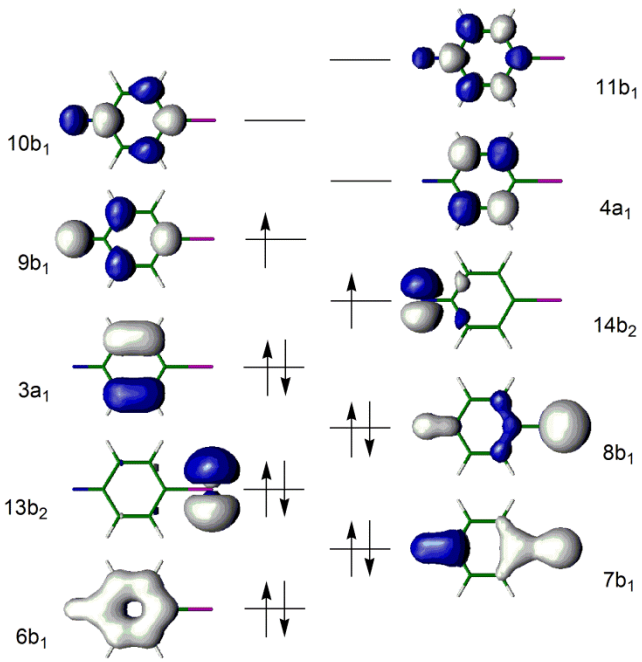

Fig. 4 CASSCF active space and the orbital occupancies in the main configuration of the 1 $^3A_2$ ground state of **12**.

The present calculations overestimate the D^{SS+SO} values by 10–20%, but the *D* values is sufficiently reproduced. The D^{SS} value is close to 1.0 cm^{-1} in **9**–**12**, and the main difference in the **D** tensors is clearly seen in the $\mathbf{D}^{SO}$ term. The D^{SO} value gradually decreases by the substitution of heavier halogen atoms. The important excited states of **9**–**12** of which the $\mathbf{D}^{SO}$ contributions are larger than 0.01 cm^{-1} in the absolute values are summarized in Tables 7–10, respectively. Similar to the case of trinitrenopyridines, the (SOMO → SOMO) spin flip excited singlet states dominantly contribute to the $\mathbf{D}^{SO}$ tensor in the fluorine derivative **9**, and the $\mathbf{D}^{SO}$ contributions from the (lone

pair → SOMO) and (lone pair → π*) excited states increase in heavier halogen derivatives. The (lone pair → SOMO) excited singlet and triplet states have very large SOCCs in the iodine derivative **12**, and the D^{SO}_{zz} contribution amounts to 2.5623 cm^{-1} and −2.6495 cm^{-1} for 3 $^1A_1$ and 2 $^3A_1$ states, respectively. Because these singlet and triplet excited states contain similar electron configurations, which give contributions to $\mathbf{D}^{SO}$ similarly in magnitude with different signs. As a result, a large amount of the $\mathbf{D}^{SO}$ contributions from these excited states is cancelled out. Similar tendency is also seen in the (lone pair → π*) excited states.

We also carried out the DFT calculations of the $\mathbf{D}^{SO}$ tensor of **9**–**12** at the UBP86/Sapporo-DZP-2012 level using the PK, CP, and QRO approaches. Among three approaches only the PK method reproduces the trends of the D^{SO} values of our hybrid method (**9** > **10** > **11** > **12**). However, the magnitude of the $D^{SO}_{PK\text{-}BP86}$ is roughly 20 times larger than the D^{SO}_{hybrid} value, and the D^{SO}_{ZZ} axes of **11** and **12** do not coincide with those calculated by the hybrid CASSCF/MRMP2. The calculated result clearly shows that all of the PK/CP/QRO DFT-based approaches to the $\mathbf{D}^{SO}$ tensor are inadequate to reproduce the heavy atom effects on nitrenes. In this context, we emphasize that the improvement of the DFT-based approaches cannot be overestimated for their further development.

Analysis of the $\mathbf{D}^{SO}$ tensors calculated at PK-DFT on the basis of an orbital region partitioning.

Among the three DFT-based approaches for $\mathbf{D}^{SO}$ tensors, the PK method gives the smallest error compared with the hybrid CASSCF/MRMP2 results. The working equation of the PK method is given in eqn (4).

$$
\begin{aligned}
D^{SO}_{kl}(\mathrm{PK}) = &-\frac{1}{4S^2}\sum_{i\alpha}^{occ}\sum_{a\alpha}^{vir}\frac{\langle\varphi_{i\alpha}|h^k|\varphi_{a\alpha}\rangle\langle\varphi_{a\alpha}|h^l|\varphi_{i\alpha}\rangle}{\varepsilon_{a\alpha}-\varepsilon_{i\alpha}} \\
&-\frac{1}{4S^2}\sum_{i\beta}^{occ}\sum_{a\beta}^{vir}\frac{\langle\psi_{i\beta}|h^k|\psi_{a\beta}\rangle\langle\psi_{a\beta}|h^l|\psi_{i\beta}\rangle}{\varepsilon_{a\beta}-\varepsilon_{i\beta}} \\
&+\frac{1}{4S^2}\sum_{i\alpha}^{occ}\sum_{a\beta}^{vir}\frac{\langle\varphi_{i\alpha}|h^k|\psi_{a\beta}\rangle\langle\psi_{a\beta}|h^l|\varphi_{i\alpha}\rangle}{\varepsilon_{a\beta}-\varepsilon_{i\alpha}} \\
&+\frac{1}{4S^2}\sum_{i\beta}^{occ}\sum_{a\alpha}^{vir}\frac{\langle\psi_{i\beta}|h^k|\varphi_{a\alpha}\rangle\langle\varphi_{a\alpha}|h^l|\psi_{i\beta}\rangle}{\varepsilon_{a\alpha}-\varepsilon_{i\beta}} \qquad (4)
\end{aligned}
$$

Here, the spatial parts of α and β spin orbitals are denoted by φ and ψ, respectively, and the occupied and unoccupied spatial orbitals labelled by *i* and *a*, respectively. The orbital energies are denoted by ε. So far, the analysis of the theoretical $\mathbf{D}^{SO}$ tensors by means of PK-DFT was carried out on the basis of the spin configurations (α → α, β → β, α → β, and β → α).[22,30,33,36] However, this type of analysis is not always useful, because the $\mathbf{D}^{SO}$ contribution from each spin configuration is generally much larger in magnitude than the $\mathbf{D}^{SO}$ tensor itself. The decomposed $\mathbf{D}^{SO}$ tensor of **3** based on the spin configuration at the UBP86/cc-pVDZ level is given in Table 11 as a representative example. It is hard to say which excitation is responsible for the positive D^{SO} value of **3**, because most of the $\mathbf{D}^{SO}$ contributions are cancelled out.

Table 11. The decomposed $\mathbf{D}^{SO}$ tensor of **3** on the basis of spin configurations.

Excitations	D_{xx}/cm^{-1}	D_{yy}/cm^{-1}	D_{zz}/cm^{-1}
α → α	−27.30504	−22.17035	−25.65662
β → β	−27.05575	−24.20433	−26.19113
α → β	27.17867	24.77412	26.83483
β → α	27.16068	21.79263	24.96313

Instead, we propose the $\mathbf{D}^{SO}$ analysis based on the orbital region partitioning. At first, we define "most similar" pairs of α and β spin orbitals having the largest $<\varphi_\alpha|\psi_\beta>$ overlap. Then, each orbital pair is assigned to three regions (doubly occupied region (DOR), singly occupied region (SOR), and unoccupied region (UOR)) in terms of the occupation number as illustrated in Fig. 5. According to this region partitioning, the $\mathbf{D}^{SO}$ tensor can be decomposed into four contributions: DOR → UOR, SOR → UOR, DOR → SOR and SOR → SOR. The relationship between the excitation patterns in the orbital region partitioning and spin configurations is summarized in Table 12. To perform this analysis we implemented a PK-DFT program code in GAMESS-US software. In our implementation, the SOC integrals are evaluated using one-electron spin–orbit Hamiltonian with effective nuclear charges. We choose the bromo derivative **3** as an example. At the UBP86/cc-pVDZ level of calculation, the D^{SO} value is calculated to be +0.2277 cm^{-1}. The decomposed $\mathbf{D}^{SO}$ tensor of **3** based on the orbital region partitioning is given in Table 13. The spin configuration-based and the orbital region partitioning-based $\mathbf{D}^{SO}$ tensor analyses of other compounds are given in ESI.†

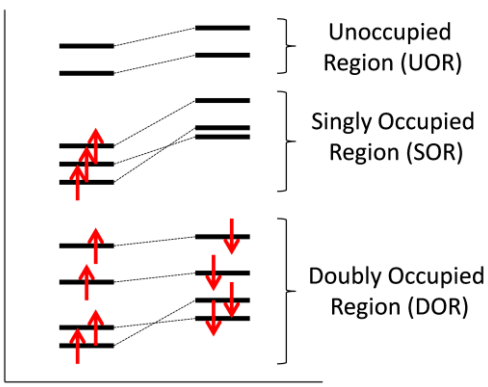

Fig. 5 Schematic representation of the definitions of the orbital region partitioning for the analysis of the $\mathbf{D}^{SO}$ tensors calculated by PK-DFT.

Table 12. Relationship between orbital region partitioning and spin configurations

Type of excitations	Conceivable spin configurations
DOR → UOR	α → α, β → β, α → β, β → α
SOR → UOR	α → α, α → β
DOR → SOR	α → β, β → β
SOR → SOR	α → β

Table 13. The decomposed $\mathbf{D}^{SO}$ tensor of **3** on the basis of the orbital region partitioning.

Excitations	D_{xx}/cm^{-1}	D_{yy}/cm^{-1}	D_{zz}/cm^{-1}
DOR → UOR	0.05645	0.03028	0.04930
SOR → UOR	−0.06956	−0.04605	−0.11000
DOR → SOR	−0.03288	−0.54027	−0.09153
SOR → SOR	0.02455	0.74811	0.10245

According to the orbital region partitioning, the large $D^{SO}{}_{yy}$ value and hence the positive D^{SO} value given by PK-DFT arises from the SOR → SOR excitations. Note that in the hybrid CASSCF/MRMP2 calculations the $D^{SO}{}_{yy}$ value from the spin-quintet excited states is 0.0602 cm^{-1} and roughly 12 times smaller than the (SOR → SOR) value of PK-DFT. Frontier orbitals of **3** calculated at UBP86/cc-pVDZ are illustrated in Fig. S1 in ESI†. The Kohn–Sham orbitals of **3** within SOR have large amplitude on the substituted bromine atoms, and thus giving strong SOCs.

A prediction of the ZFS parameters of 3,5-diiodo-2,4,6-trinitrenopyridine 13.

Recently, Chapyshev and Chernyak reported organic synthesis of 2,4,6-triazido-3,5-diiodopyridine **4-I**,[91] that can be a precursor of 3,5-diiodo-2,4,6-trinitrenopyridine **13**. Although the generation of trinitrene **13** has not been reported to our knowledge, it is worthwhile to predict the $\mathbf{D}^{SO}$ tensor of **13** prior to ESR experiments. We used DZVP basis set for the geometry optimization by using HCTH/407 functional, and CASSCF(20e,16o) and MRMP2 calculations. According to the hybrid method, the D^{SO} and E^{SO} values of **13** are calculated to be −0.3431 cm^{-1} and −0.0635 cm^{-1}, respectively. The $D^{SO}{}_{ZZ}$ axis is parallel to the direction connecting the two iodine atoms. The D^{SS} and E^{SS} values are calculated to be −0.1068 cm^{-1} and −0.0100 cm^{-1}, respectively. The resultant D^{SS+SO} and E^{SS+SO} values are −0.3046 cm^{-1} and −0.0051 cm^{-1}, respectively. Similarly to **3** the (lone pair → SOMO) excited states dominantly contribute the negative D^{SO} value of **13**.

4. Conclusions

In the present study, the $\mathbf{D}^{SS}$ and $\mathbf{D}^{SO}$ tensors of halogen-substituted 2,4,6-trinitrenopyridines **1**–**3** and *p*-phenylnitrenes **9**–**12** have been calculated by the CASSCF and the hybrid CASSCF/MRMP2 methods. The calculations reproduced trends of the experimental $|D|$ values, and the theoretical D^{SS+SO} values agreed with the experiment with an error of less than 15%.

The $\mathbf{D}^{SS}$ tensors are hardly perturbed by the introduction of halogen substituents. By contrast, the $\mathbf{D}^{SO}$ tensors are strongly influenced by the halogen substitutions. The introduction of heavier halogen atoms causes negative shifts of the principal values of $\mathbf{D}^{SO}$. The positive $\mathbf{D}^{SO}$ contributions from the (SOMO → SOMO) spin flip excited states of $\sigma = -1$ are less sensitive to halogen substitutions, but the (lone pair → SOMO) excited states of the same spin multiplicity as the ground state ($\sigma = 0$) give rise to the large negative $\mathbf{D}^{SO}$ contributions in the heavier halogen derivatives. The $\mathbf{D}^{SO}$ contributions from the excited quintet and septet states are comparable in magnitude with different signs in **2**, and the $\mathbf{D}^{SO}$ contributions from the excited septet states become predominant in **3**. In bromo- and iodo-substituted compounds **3**, **11**, and **12**, the (lone pair → π*) excited states of $\sigma = +1$ have large SOCCs and therefore non-negligible contributions to the $\mathbf{D}^{SO}$ tensor, in spite of high excitation energies of these states.

The comparison between theoretical $\mathbf{D}^{SO}$ tensors calculated by the hybrid CASSCF/MRMP2 method and the PK/CP/QRO-DFT methods revealed that all the tested DFT-based methods are inadequate to investigate the heavy atom effects on ZFS of the molecules under study. In order to analyze origins of the error in PK-DFT, we have introduced an approach of orbital region partitioning, which is based on the occupation number of α–β orbital pairs. The orbital region partitioning analysis revealed that the large positive D^{SO} value of **3** obtained by PK-DFT arises from the strong delocalization of SOMOs onto the bromine atoms.

Finally, the **D** tensor of 3,5-diiodo-2,4,6-trinitrenopyridine **13**, which can afford a test bed for the theory of $\mathbf{D}^{SO}$ tensors, is predicted. We encourage experimentalists to give the experimentally determined **D** tensor of **13** and those of other related iodine-substituted nitrenes.

In quest for new molecular spin functionalities and their control, molecular optimization becomes crucial. In this context, the control of SOC in D tensors is important. In this work, we emphasize that the DFT-based theoretical calculations for the $\mathbf{D}^{SS}$ and $\mathbf{D}^{SO}$ tensors have attracted attention owing to their low computational costs and the availability of the published quantum chemistry program packages[70,71] and at the same time we notice that some difficulties intrinsic to the DFT-based approaches have been pointed out by several groups[23–31] and sophisticated ab initio methods usually give more reliable results than DFT. Thus, the improvement of the DFT-based approaches is extremely important for their further development and applications to sizable molecular systems.

Acknowledgements

This work has been supported by Grants-in-Aid for Scientific Research on Innovative Areas "Quantum Cybernetics" and Scientific Research (B) from MEXT, Japan. The support for the present work by the FIRST project on "Quantum Information Processing" from JSPS, Japan and by the AOARD project on "Quantum Properties of Molecular Nanomagnets" (Award No. FA2386-13-1-4030) is also acknowledged.

Notes and references

[a] *Department of Chemistry, Graduate School of Science, Osaka City University, 3-3-138 Sugimoto, Sumiyoshi-ku, Osaka 558-8585, Japan. E-mail: toyota@sci.osaka-cu.ac.jp, sato@sci.osaka-cu.ac.jp, takui@sci.osaka-cu.ac.jp*

[b] *Department of System Innovation, Graduate School of Engineering Science, Osaka University, 1-3 Machikaneyama, Toyonaka, Osaka 560-8531, Japan*

† Electronic Supplementary Information (ESI) available: Cartesian coordinates, absolute energies and $\langle S^2 \rangle$ values of **1**–**3** and **9**–**13**, DFT-based $\mathbf{D}^{SO}$ tensor calculations of **1**–**3**, UBP86/cc-pVDZ frontier orbitals of **3**, and spin configuration-based and orbital region partitioning-based analyses of the $\mathbf{D}^{SO}$ tensors of **1**,**2**, and **9**–**13** calculated at PK-DFT. See DOI: 10.1039/b000000x/

1 T. Bally, in *Reactive Intermediates Chemistry*, ed. R. A. Moss, M. S. Platz and M. Jones Jr., Wiley Interscience, New Jersey, 2004, ch. 17, pp. 797–845.

2 A. Mardyukov and W. Sander, in *Encyclopedia of Radicals in Chemistry, Biology and Materials*, ed. C. Chatgilialoglu and C. Studer, Wiley, 2012, ch. 9, pp. 207–228.

3 K. Sato, D. Shiomi, T. Takui, K. Itoh, T. Kaneko, E. Tsuchida and H. Nishide, *J. Spectrosc. Soc. Jpn.*, 1994, **43**, 280–291.

4 K. Sato, M. Yano, M. Furuichi, D. Shiomi, T. Takui, K. Abe, K. Itoh, A. Higuchi, K. Katsuma and Y. Shirota, *J. Am. Chem. Soc.*, 1997, **119**, 6607–6613.

5 J. Isoya, H. Kanda, J. R. Norris J. Tang and M. K. Bowman, *Phys. Rev. B*, 1990, **41**, 3905–3913.

6 A. V. Astashkin and A. Schweiger, *Chem. Phys. Lett.*, 1990, **174**, 595–602.

7 H. Tomioka, T. Watanabe, K. Hirai, K. Furukawa, T. Takui and K. Itoh, *J. Am. Chem. Soc.*, 1995, **117**, 6376–6377.

8 M. C. B. L. Shohoji, M. L. T. M. B. Franco, C. R. L. R. Lazana, S. Nakazawa, K. Sato, D. Shiomi and T. Takui, *J. Am. Chem. Soc.*, 2000, **122**, 2962–2963.

9 T. Sawai, K. Sato, T. Ise, D. Shiomi, K. Toyota, T. Morita and T. Takui, *Angew. Chem. Int. Ed.*, 2008, **47**, 3988–3990.

10 S. Nakazawa, K. Sato, D. Shiomi, M. Yano, T. Kinoshita, M. L. T. M. B. Franco, M. C. R. L. R. Lazana, M. C. B. L. Shohoji, K. Itoh and T. Takui, *Phys. Chem. Chem. Phys.*, 2011, **13**, 1424–1433.

11 K. Ayabe, K. Sato, S. Nishida, T. Ise, S. Nakazawa, K. Sugisaki, Y. Morita, K. Toyota, D. Shiomi, M. Kitagawa and T. Takui, *Phys. Chem. Chem. Phys.*, 2012, **14**, 9137–9148.

12 K. Ayabe, K. Sato, S. Nakazawa, S. Nishida, K. Sugisaki, T. Ise, Y. Morita, K. Toyota, D. Shiomi, M. Kitagawa, S. Suzuki, K. Okada and T. Takui, *Mol. Phys.*, 2013, **111**, 2767–2787.

13 T. Takui, K. Sato, D. Shiomi and K. Itoh, in *Magnetic Properties of Organic Materials*, ed. P. M. Lahti, Marcel Dekker Inc., Amsterdam, 1999, ch. 11, pp. 197–236.

14 K. Sato, *Dr thesis*, Osaka City University, 1994.

15 C. N. Banwell and H. Primas, *Mol. Phys.*, 1963, **6**, 225–256.

16 G. G. Belford, R. L. Belford and J. F. Burkhalter, *J. Magn. Reson.*, 1973, **11**, 251–265.

17 K. T. McGregor, R. P. Scaringe and W. E. Hatfield, *Mol. Phys.*, 1975, **30**, 1925–1933.

18 K. Sugisaki, K. Toyota, K. Sato, D. Shiomi, M. Kitagawa and T. Takui, in *EPR of Free Radicals in Solids I, Progress in Theoretical Chemistry and Physics Vol. 24*, Springer, Dordrecht, 2013, ch. 8, pp. 363–392.

19 J. E. Harriman, *Theoretical Foundations of Electron Spin Resonance*, Academic Press, New York, 1978.

20 M. R. Pederson and S. N. Khanna, *Phys. Rev. B*, 1999, **60**, 9566–9572.

21 F. Neese, *J. Chem. Phys.*, 2007, **127**, 164112.

22 F. Neese, *J. Am. Chem. Soc.*, 2006, **128**, 10213–10222.

23 S. Sinnecker and F. Neese, *J. Phys. Chem. A*, 2006, **110**, 12267–12275.

24 C. van Wüllen, *J. Chem. Phys.*, 2009, **130**, 194109.

25 C. van Wüllen, *J. Phys. Chem. A*, 2009, **113**, 11535–11540.

26 S. Schmitt, P. Jost and C. van Wüllen, *J. Chem. Phys.*, 2011, **134**, 194113.

27 K. Sugisaki, K. Toyota, K. Sato, D. Shiomi, M. Kitagawa and T. Takui, *Chem. Phys. Lett.*, 2009, **477**, 369–373.

28 K. Sugisaki, K. Toyota, K. Sato, D. Shiomi, M. Kitagawa and T. Takui, *ChemPhysChem*, 2010, **11**, 3146–3151.

29 K. Sugisaki, K. Toyota, K. Sato, D. Shiomi, M. Kitagawa and T. Takui, *Phys. Chem. Chem. Phys.*, 2011, **13**, 6970–6980.

30 A. Kubica, J. Kowalewski, D. Kruk and M. Odelius, *J. Chem. Phys.*, 2013, **138**, 064304.

31 P. Jost and C. van Wüllen, *Phys. Chem. Chem. Phys.*, 2013, **15**, 16426–16427.

32 D. Ganyushin and F. Neese, *J. Chem. Phys.*, 2006, **125**, 024103.

33 C. Duboc, T. Phoeung, S. Zein, J. Pécaut, M.-N. Collomb and F. Neese, *Inorg. Chem.*, 2007, **46**, 4905–4916.

34 S. Zein and F. Neese, *J. Phys. Chem. A*, 2008, **112**, 7976–7983.

35 D. G. Liakos, D. Ganyushin and F. Neese, *Inorg. Chem.*, 2009, **48**, 10572–10580.

36 S. Ye, F. Neese, A. Ozarowski, D. Smirnov, J. Krzystek, J. Telser, J.-H. Liao, C.-H. Hung, W.-C. Chu, Y.-F. Tsai, R.-C. Wang, K.-Y. Chen and H.-F. Hsu, *Inorg. Chem.*, 2010, **49**, 977–988.

37 S. Ye and F. Neese, *J. Chem. Theory Comput.*, 2012, **8**, 2344–2351.

38 F. Aquino and J. H. Rodriguez, *J. Chem. Phys.*, **2005**, *123*, 204902.

39 R. Reviakine, A. V. Arbuznikov, J.-C. Tremblay, C. Remenyi, O. L. Malkina, V. G. Malkin and M. Kaupp, *J. Chem. Phys.*, 2006, **125**, 054110.

40 R. Takeda, M. Shoji, S. Yamanaka and K. Yamaguchi, *Polyhedron*, 2005, **24**, 2238–2241.

41 R. Takeda, K. Koizumi, M. Shoji, H. Nitta, S. Yamanaka, M. Okumura and K. Yamaguchi, *Polyhedron*, 2007, **26**, 2309–2312.

42 M. Shoji, K. Koizumi, T. Hamamoto, T. Taniguchi, R. Takeda, Y. Kitagawa, T. Kawakami, M. Okumura, S. Yamanaka and K. Yamaguchi, *Polyhedron*, 2005, **24**, 2708–2715.

43 W. Sander, D. Grote, S. Kossmann and F. Neese, *J. Am. Chem. Soc.*, 2008, **130**, 4396–4403.

44 D. Grote, C. Finke, S. Kossmann, F. Neese and W. Sander, *Chem. Eur. J.*, 2010, **16**, 4496–4506.

45 P. Neuhaus, M. Winkler and W. Sander, *J. Phys. Org. Chem.*, 2011, **24**, 976–992.

46 E. Y. Misochko, D. V. Korchagin, K. V. Bozhenko, S. V. Chapyshev and S. M. Aldoshin, *J. Chem. Phys.*, 2010, **133**, 064101.

47 E. Y. Misochko, A. V. Akimov, A. A. Masitov, D. V. Korchagin, S. M. Aldoshin, S. E. Boganov, K. N. Shavrin, V. D. Gvozdev, M. P. Egorov and O. M. Nefedov, *Russ. Chem. Bull. Int. Ed.*, 2011, **60**, 2180–2187.

48 T. Koto, K. Sugisaki, K. Sato, D. Shiomi, K. Toyota, K. Itoh, E. Wasserman, P. M. Lahti and T. Takui, *Appl. Magn. Reson.*, 2010, **37**, 703–736.

49 S. V. Chapyshev, D. V. Korchagin, M. F. Budyka, T. N. Gavrishova, P. Neuhaus and W. Sander, *J. Phys. Chem. A*, 2011, **115**, 8419–8425.

50 E. Y. Misochko, A. V. Akimov, D. V. Korchagin, A. A. Masitov and K. N. Shavrin, *Phys. Chem. Chem. Phys.*, 2012, **14**, 2032–2039.

51 S. S. R. R. Perumal, *Chem. Phys. Lett.*, 2011, **501**, 608–611.

52 Z. Havlas, M. Kývala and J. Michl, *Collect. Czech. Chem. Commun.*, 2003, **68**, 2335–2343.

53 Z. Havlas, M. Kývala and J. Michl, *Mol. Phys.*, 2005, **103**, 407–411.

54 O. Vahtras, O. Loboda, B. Minaev, H. Ågren and K. Ruud, *Chem. Phys.*, 2002, **279**, 133–142.

55 O. Loboda, B. Minaev, O. Vahtras, B. Schimmelpfennig, H. Ågren, K. Ruud and D. Jonsson, *Chem. Phys.*, 2003, **286**, 127–137.

56 O. Loboda, B. Minaev, O. Vahtras, K. Ruud and H. Ågren, *J. Chem. Phys.*, 2003, **119**, 3120–3129.

57 B. Minaev, O. Loboda, O. Vahtras, K. Ruud and H. Ågren, *Theor. Chem. Acc.*, 2004, **111**, 168–175.

58 Ò. Rubio-Pons, B. Minaev, O. Loboda and H. Ågren, *Theor. Chem. Acc.*, 2005, **113**, 15–27.

59 B. F. Minaev, E. M. Khomenko, E. A .Bilan and L. B. Yashchuk, *Opt. Spectrosc.*, 2005, **98**, 209–213.

60 S. S. R. R. Perumal, B. Minaev and H. Ågren, *J. Chem. Phys.*, 2012, **136**, 104702.

61 S. Ye and F. Neese, *J. Chem. Theory Comput.*, 2012, **8**, 2344–2351.

62 R. Maurice, A. M. Pradipto, N. Guihery, R. Broer and C. de Graaf, *J. Chem. Theory Comput.*, 2010, **6**, 3092–3101.

63 N. Gilka, P. R. Taylor and C. M. Marian, *J. Chem. Phys.*, 2008, **129**, 044102.

64 J.-B. Rota, S. Knecht, T. Fleig, D. Ganyushin, T. Saue, F. Neese and H. Bolvin, *J. Chem. Phys.*, 2011, **135**, 114106.

65 C. de Graaf and C. Sousa, *Int. J. Quantum Chem.*, 2006, **106**, 2470–2478.

66 R. Maurice, R. Bastardis, C. de Graaf, N. Suaud, T. Mallah and N. Guihéry, *J. Chem. Theory Comput.*, 2009, **5**, 2977–2984.

67 B. Minaev, L. Yaschuk and V. Kukueva, *Spectrochim. Acta A*, 2005, **61**, 1105–1112.

68 T. Yoshizawa and T. Nakajima, *Chem. Phys. Lett.*, 2011, **515**, 296–301.

69 T. Yoshizawa and T. Nakajima, *Chem. Phys. Lett.*, 2012, **549**, 108–112.

70 F. Neese, *ORCA, an ab initio, density functional and semiempirical program package*, University of Bonn, Germany.
71 *ADF2012*, SCM, Theoretical Chemistry, Vrije Universiteit, Amsterdam, The Netherlands, http://www.scm.com
72 K. Hirao, *Chem. Phys. Lett.*, 1992, **190**, 374–380.
73 K. Hirao, *Chem. Phys. Lett.*, 1992, **196**, 397–403.
74 K. Hirao, *Chem. Phys. Lett.*, 1993, **201**, 59–66.
75 X. Zhu, S. Saito, A. Kemp, K. Kakuyanagi, S. Karimoto, H. Nakano, W. J. Munro, Y. Tokura, M. S. Everitt, K. Nemoto, M. Kasu, N. Mizuochi and K. Semba, *Nature*, 2011, **478**, 221–224.
76 E. Wasserman, *Prog. Phys. Org. Chem.*, 1971, **8**, 319–336.
77 J. A. Hebden and C. A. McDowell, *J. Magn. Reson.*, 1971, **5**, 115–133.
78 A. S. Ichimura, K. Sato, T. Kinoshita, T. Takui, K. Itoh and P. M. Lahti, *Mol. Cryst. Liq. Cryst.*, 1995, **272**, 57–66.
79 S. V. Chapyshev, D. Grote, C. Finke and W. Sander, *J. Org. Chem.*, 2008, **73**, 7045–7051.
80 E. Y. Misochko, A. V. Akimov and S. V. Chapyshev, *J. Chem. Phys.*, 2008, **129**, 174510.
81 S. V. Chapyshev, P. Neuhaus, D. Grote and W. Sander, *J. Phys. Org. Chem.*, 2010, **23**, 340–346.
82 E. Y. Misochko, A. V. Akimov, A. A. Masitov, D. V. Korchagin, I. K. Yakushchenko and S. V. Chapyshev, *J. Chem. Phys.*, 2012, **137**, 064308.
83 M. J. Frisch, G. W. Trucks, H. B. Schlegel, G. E. Scuseria, M. A. Robb, J. R. Cheeseman, G. Scalmani, V. Barone, B. Mennucci, G. A. Petersson, H. Nakatsuji, M. Caricato, X. Li, H. P. Hratchian, A. F. Izmaylov, J. Bloino, G. Zheng, J. L. Sonnenberg, M. Hada, M. Ehara, K. Toyota, R. Fukuda, J. Hasegawa, M. Ishida, T. Nakajima, Y. Honda, O. Kitao, H. Nakai, T. Vreven, J. A. Montgomery, Jr., J. E. Peralta, F. Ogliaro, M. Bearpark, J. J. Heyd, E. Brothers, K. N. Kudin, V. N. Staroverov, R. Kobayashi, J. Normand, K. Raghavachari, A. Rendell, J. C. Burant, S. S. Iyengar, J. Tomasi, M. Cossi, N. Rega, J. M. Millam, M. Klene, J. E. Knox, J. B. Cross, V. Bakken, C. Adamo, J. Jaramillo, R. Gomperts, R. E. Stratmann, O. Yazyev, A. J. Austin, R. Cammi, C. Pomelli, J. W. Ochterski, R. L. Martin, K. Morokuma, V. G. Zakrzewski, G. A. Voth, P. Salvador, J. J. Dannenberg, S. Dapprich, A. D. Daniels, O, Farkas, J. B. Foresman, J. V. Ortiz, J. Cioslowski and D. J. Fox, *GAUSSIAN 03 (Revision D.01)*, Gaussian Inc., Wallingford CT, 2004.
84 *Dalton, a molecular electronic structure program*, Release Dalton2011, see http://daltonprogram.org/
85 F. Neese and E. I. Solomon, *Inorg. Chem.*, 1998, **37**, 6568–6582.
86 Y.-K. Choe, H. A. Witek, J. P. Finley and K. Hirao, *J. Chem. Phys.*, 2001, **114**, 3913–3918.
87 H. A. Witek, D. G. Fedorov and K. Hirao, *J. Comput. Chem.*, 2002, **23**, 957–965.
88 M. W. Schmidt, K. K. Baldridge, J. A. Boatz, S. T. Elbert, M. S. Gordon, J. H. Jensen, S. Koseki, N. Matsunaga, K. A. Nguyen, S. J. Su, T. L. Windus, M. Dupuis and J. A. Montgomery, *J. Comput. Chem.*, 1993, **14**, 1347–1363.
89 J. H. Hall, J. M. Fargher and M. R. Gisler, *J. Am. Chem. Soc.*, 1978, **100**, 2029–2034.
90 T. Noro, M. Sekiya and T. Koga, *Theor. Chem. Acc.*, 2012, **131**, 1124.
91 S. V. Chapyshev and A. V. Chernyak, *Synthesis*, 2012, **44**, 3158–3160.

Table 1 Experimental and theoretical ZFS parameters D and E of spin-septet trinitrenes **1**–**3**.

Molecule	D^{SS}/cm^{-1}	D^{SO}/cm^{-1}	D^{SS+SO}/cm^{-1}	$\|D$(Exptl.)$\|$/cm^{-1}	$D^{SO}_{PK\text{-}PBE}$[82]/cm^{-1}	E^{SS}/cm^{-1}	E^{SO}/cm^{-1}	E^{SS+SO}/cm^{-1}	$\|E$(Exptl.)$\|$/cm^{-1}
1	−0.1035	−0.0124	−0.1159	0.1018[79]	−0.007	−0.0042	+0.0001	−0.0041	0.0037[79]
2	−0.1011	+0.0065	−0.1055[a]	0.1019[80]	+0.013	−0.094	−0.0011	−0.0150	0.00325[80]
3	−0.1019	−0.2537	−0.2539[a]	0.297[82]	+0.194	−0.0106	−0.0260	+0.0302	0.017[82]

[a] The D_{ZZ} principal axis of $\mathbf{D}^{SO}$ does not coincide with that of $\mathbf{D}^{SS}$.

Table 2 Principal values of the theoretical $\mathbf{D}^{SS}$ and $\mathbf{D}^{SO}$ tensors of **1**–**3**. Values in boldface are the D_{ZZ} principal values in the conventional definition.

	1			**2**			**3**		
	D_{xx}/cm^{-1}	D_{yy}/cm^{-1}	D_{zz}/cm^{-1}	D_{xx}/cm^{-1}	D_{yy}/cm^{-1}	D_{zz}/cm^{-1}	D_{xx}/cm^{-1}	D_{yy}/cm^{-1}	D_{zz}/cm^{-1}
$\mathbf{D}^{SS}$	**−0.0690**	0.0303	0.0387	**−0.0674**	0.0243	0.0431	**−0.0679**	0.0234	0.0445
$\mathbf{D}^{SO}_{Quintet}$[a]	0.0000	0.0135	0.0137	0.0000	0.0149	0.0147	0.0000	0.0602	0.0193
$\mathbf{D}^{SO}_{Septet}$[b]	0.0000	−0.0011	−0.0014	0.0000	−0.0224	−0.0051	0.0000	−0.4008	−0.0766
$\mathbf{D}^{SO}_{Nonet}$[c]	0.0000	0.0007	0.0000	0.0000	0.0022	0.0004	0.0000	0.0255	0.0052
$\mathbf{D}^{SO}$(Total)	**0.0000**	0.0131	0.0123	0.0000	−0.0053	**0.0100**	0.0000	**−0.3150**	−0.0522
$\mathbf{D}^{SS+SO}$	**−0.0690**	0.0434	0.0510	**−0.0674**	0.0190	0.0531	−0.0679	**−0.2917**	−0.0076

[a] $\mathbf{D}^{SO}$ contributions from excited quintet states. [b] $\mathbf{D}^{SO}$ contributions from excited septet states. [c] $\mathbf{D}^{SO}$ contributions from excited nonet states.

Table 3 Selected electronic excited states of **1**.

	Main configurations ($\|C\| > 0.3$)[a]				D^{SO}_{ii}/cm^{-1}	
State	C[b]	Character[c]	ΔE_{MRMP2}/cm^{-1}	SOCC[d]/cm^{-1}	$i = y$	$i = z$
$3\ ^5A_1$	0.50	$14b_2 \rightarrow 4b_1$ (SOMO → SOMO)	20 477	25.71		0.0065
	0.38	$3a_2 \rightarrow 19a_1$ (SOMO → SOMO)				
	0.35	$19a_1 \rightarrow 3a_2$ (SOMO → SOMO)				
$2\ ^5B_2$	0.50	$19a_1 \rightarrow 4b_1$ (SOMO → SOMO)	22 360	37.43	0.0125	
	0.39	$14b_2 \rightarrow 3a_2$ (SOMO → SOMO)				
	−0.30	$4b_1 \rightarrow 19a_1$ (SOMO → SOMO)				
$4\ ^5A_1$	0.55	$13b_2 \rightarrow 5b_1$ (SOMO → SOMO)	22 546	26.34		0.0062
	−0.41	$14b_2 \rightarrow 5b_1$ (SOMO → SOMO)				
	−0.39	$5b_1 \rightarrow 13b_2$ (SOMO → SOMO)				
$3\ ^7A_1$	0.49	$14b_2 \rightarrow 6b_1$ (SOMO → π*)	54 754	22.09		−0.0010
	−0.47	$13b_2 \rightarrow 6b_1$ (SOMO → π*)				

[a] The active space consists of 16 orbitals: $18a_1$–$19a_1$, $1a_2$–$4a_2$, $1b_1$–$7b_1$, and $12b_2$–$14b_2$. [b] CAS-CI coefficients. [c] Excitation configurations from the main configuration of the $1\ ^7A_2$ ground state. [d] Spin–orbit coupling constants.

Table 4 Selected electronic excited states of **2**.

State	Main configurations ($\|C\| > 0.3$)[a] C[b]	Character[c]	ΔE_{MRMP2}/cm^{-1}	SOCC[d]/cm^{-1}	D^{SO}_{ii}/cm^{-1} $i = y$	$i = z$
$3\ ^5A_1$	0.47	$17b_2 \rightarrow 5b_1$ (SOMO → SOMO)	20 905	24.94		0.0060
	0.39	$4a_2 \rightarrow 22a_1$ (SOMO → SOMO)				
	0.34	$22a_1 \rightarrow 4a_2$ (SOMO → SOMO)				
$4\ ^5A_1$	0.51	$16b_2 \rightarrow 6b_1$ (SOMO → SOMO)	21 608	29.23		0.0079
	−0.42	$17b_2 \rightarrow 6b_1$ (SOMO → SOMO)				
	−0.41	$6b_1 \rightarrow 16b_2$ (SOMO → SOMO)				
$2\ ^5B_2$	0.47	$22a_1 \rightarrow 5b_1$ (SOMO → SOMO)	22 169	38.51	0.0134	
	0.38	$17b_2 \rightarrow 4a_2$ (SOMO → SOMO)				
	−0.33	$5b_1 \rightarrow 22a_1$ (SOMO → SOMO)				
$3\ ^5B_2$	0.50	$4a_2 \rightarrow 16b_2$ (SOMO → SOMO)	24 891	11.54	0.0011	
	0.31	$4a_2 \rightarrow 17b_2$ (SOMO → SOMO)				
$1\ ^7B_2$	0.71	$21a_1 \rightarrow 6b_1$ (lone pair → SOMO)	31 999	71.79	−0.0179	
	0.44	$15b_2 \rightarrow 4a_2$ (lone pair → SOMO)				
$1\ ^7A_1$	0.60	$21a_1 \rightarrow 4a_2$ (lone pair → SOMO)	33 761	29.25		−0.0028
	0.58	$15b_2 \rightarrow 6b_1$ (lone pair → SOMO)				
$4\ ^7B_2$	0.54	$15b_2 \rightarrow 4a_2$ (lone pair → SOMO)	42 938	32.39	−0.0027	
	−0.43	$21a_1 \rightarrow 6b_1$ (lone pair → SOMO)				
	0.34	$21a_1 \rightarrow 5b_1$ (lone pair → SOMO)				
$5\ ^7A_1$	0.49	$17b_2 \rightarrow 7b_1$ (SOMO → π*)	52 996	28.50		−0.0017
	−0.45	$16b_2 \rightarrow 7b_1$ (SOMO → π*)				
$2\ ^9B_2$	0.80	$15b_2 \rightarrow 5a_2$ (lone pair → π*)	67 939	28.01	0.0016	

[a] The active space consists of 16 orbitals: $21a_1$–$22a_1$, $2a_2$–$5a_2$, $2b_1$–$8b_1$, and $15b_2$–$17b_2$. [b] CAS-CI coefficients. [c] Excitation configurations from the main configuration of the $1\ ^7A_2$ ground state. [d] Spin–orbit coupling constants.

Table 5 Selected electronic excited states of **3**.

State	Main configurations ($\|C\| > 0.3$)[a] C[b]	Character[c]	ΔE_{MRMP2}/cm^{-1}	SOCC[d]/cm^{-1}	D^{SO}_{ii}/cm^{-1} $i = y$	$i = z$
$4\ ^5A_1$	0.50	$22b_2 \rightarrow 9b_1$ (SOMO → SOMO)	21 086	36.15		0.0124
	0.42	$9b_1 \rightarrow 22b_2$ (SOMO → SOMO)				
	−0.42	$23b_2 \rightarrow 9b_1$ (SOMO → SOMO)				
$2\ ^5B_2$	0.46	$28a_1 \rightarrow 8b_1$ (SOMO → SOMO)	21 816	45.68	0.0191	
	0.39	$23b_2 \rightarrow 7a_2$ (SOMO → SOMO)				
	−0.34	$8b_1 \rightarrow 28a_1$ (SOMO → SOMO)				
$1\ ^7B_2$	0.68	$27a_1 \rightarrow 9b_1$ (lone pair → SOMO)	23 843	255.07	−0.3032	
	0.39	$21b_2 \rightarrow 7a_2$ (lone pair → SOMO)				
	0.36	$27a_1 \rightarrow 8b_1$ (lone pair → SOMO)				
$1\ ^7A_1$	0.62	$27a_1 \rightarrow 7a_2$ (lone pair → SOMO)	24 685	126.81		−0.0724
	0.58	$21b_2 \rightarrow 9b_1$ (lone pair → SOMO)				
$2\ ^7B_2$	0.69	$27a_1 \rightarrow 8b_1$ (lone pair → SOMO)	28 775	92.57	−0.0331	
	−0.44	$21b_2 \rightarrow 7a_2$ (lone pair → SOMO)				
$5\ ^5B_2$	0.35	$23b_2 \rightarrow 7a_2$ (SOMO → SOMO)	31 611	71.15	0.0320	
$3\ ^7B_2$	0.58	$21b_2 \rightarrow 7a_2$ (lone pair → SOMO)	34 045	108.99	−0.0388	
	−0.46	$27a_1 \rightarrow 9b_1$ (lone pair → SOMO)				
$2\ ^9B_2$	0.81	$21b_2 \rightarrow 8a_2$ (lone pair → π*)	61 531	92.48	0.0199	

[a] The active space consists of 16 orbitals: $27a_1$–$28a_1$, $5a_2$–$8a_2$, $5b_1$–$11b_1$, and $21b_2$–$23b_2$. [b] CAS-CI coefficients. [c] Excitation configurations from the main configuration of the $1\ ^7A_2$ ground state. [d] Spin–orbit coupling constants.

Table 6 Experimental and theoretical ZFS parameters D of *p*-substituted phenylnitrenes **9**–**12**.

Molecule	D^{SS}/cm^{-1}	D^{SO}/cm^{-1}	D^{SS+SO}/cm^{-1}	|D(Exptl.)[89]|/cm^{-1}	$D^{SO}_{PK\text{-}BP86}$/cm^{-1}	$D^{SO}_{CP\text{-}BP86}$/cm^{-1}	$D^{SO}_{QRO\text{-}BP86}$/cm^{-1}
9	+1.0171	+0.1139	+1.1310	1.008	+0.0433	+0.1129	+0.0798
10	+0.9905	+0.0986	+1.0891	0.951	+0.0355	−0.2762	+0.2582
11	+0.9969	+0.0812	+1.0781	0.911	−0.0992	+3.1656	−8.2175
12	+0.9979	−0.0281	+0.9698	0.871	−0.5677	+21.0699	−52.3221

Table 7 Selected electronic excited states of **9**.

State	Main configurations ($\|C\| > 0.3$)[a] C[b]	Character[c]	ΔE_{MRMP2}/cm^{-1}	SOCC[d]/cm^{-1}	D^{SO}_{zz}/cm^{-1}
$1\ ^1A_1$	0.84	$4b_1 \rightarrow 9b_2$ (SOMO → SOMO)	11 324	12.62	0.0141
	−0.36	$9b_2 \rightarrow 4b_1$ (SOMO → SOMO)			
$2\ ^1A_1$	0.84	$9b_2 \rightarrow 4b_1$ (SOMO → SOMO)	23 110	46.26	0.0926
	0.34	$4b_1 \rightarrow 9b_2$ (SOMO → SOMO)			

[a] The active space consists of 10 orbitals: $1a_2$–$2a_2$, $1b_1$–$6b_1$, and $8b_2$–$9b_2$. [b] CAS-CI coefficients. [c] Excitation configurations from the main configuration of the $1\ ^3A_2$ ground state. [d] Spin–orbit coupling constants.

Table 8 Selected electronic excited states of **10**.

State	Main configurations ($\|C\| > 0.3$)[a] C[b]	Character[c]	ΔE_{MRMP2}/cm^{-1}	SOCC[d]/cm^{-1}	D^{SO}_{zz}/cm^{-1}
$1\ ^1A_1$	−0.83	$5b_1 \rightarrow 10b_2$ (SOMO → SOMO)	11 823	11.25	0.0107
	0.37	$10b_2 \rightarrow 5b_1$ (SOMO → SOMO)			
$2\ ^1A_1$	−0.83	$10b_2 \rightarrow 5b_1$ (SOMO → SOMO)	22 749	45.37	0.0905
	−0.35	$5b_1 \rightarrow 10b_2$ (SOMO → SOMO)			
$4\ ^3A_1$	0.93	$9b_2 \rightarrow 5b_1$ (lone pair → SOMO)	55 101	46.91	−0.0399
$4\ ^1A_1$	0.59	$9b_2 \rightarrow 5b_1$ (lone pair → SOMO)	56 181	30.30	0.0163
	−0.34	$10b_2 \rightarrow 6b_1$ (SOMO → π*)			
$5\ ^1A_1$	−0.65	$9b_2 \rightarrow 5b_1$ (lone pair → SOMO)	56 754	36.04	0.0229
	−0.35	$10b_2 \rightarrow 6b_1$ (SOMO → π*)			

[a] The active space consists of 10 orbitals: $1a_2$–$2a_2$, $2b_1$–$7b_1$, and $9b_2$–$10b_2$. [b] CAS-CI coefficients. [c] Excitation configurations from the main configuration of the $1\ ^3A_2$ ground state. [d] Spin–orbit coupling constants.

Table 9 Selected electronic excited states of **11**.

State	Main configurations ($\|C\| > 0.3$)[a] C[b]	Character[c]	ΔE_{MRMP2}/cm^{-1}	SOCC[d]/cm^{-1}	D^{SO}_{zz}/cm^{-1}
$2\ ^1A_1$	0.82	$12b_2 \rightarrow 7b_1$ (SOMO → SOMO)	22 637	43.10	0.0821
	0.36	$7b_1 \rightarrow 12b_2$ (SOMO → SOMO)			
$5\ ^3A_1$	0.93	$11b_2 \rightarrow 7b_1$ (lone pair → SOMO)	56 516	174.31	−0.5376
$4\ ^1A_1$	−0.87	$11b_2 \rightarrow 7b_1$ (lone pair → SOMO)	56 774	160.38	0.4531
$5\ ^1A_1$	−0.44	$12b_2 \rightarrow 8b_1$ (SOMO → π*)	57 476	43.76	0.0333
	−0.41	$6b_1 \rightarrow 12b_2$ (π → SOMO)			
$7\ ^1A_1$	0.49	$6b_1 \rightarrow 12b_2$ (π → SOMO)	59 436	46.63	0.0366
$10\ ^3A_1$	−0.81	$11b_2 \rightarrow 8b_1$ (lone pair → π*)	76 182	65.30	−0.0560
$2\ ^5A_1$	−0.91	$11b_2 \rightarrow 8b_1$ (lone pair → π*)	76 755	120.59	0.0632

[a] The active space consists of 10 orbitals: $2a_2$–$3a_2$, $4b_1$–$9b_1$, and $11b_2$–$12b_2$. [b] CAS-CI coefficients. [c] Excitation configurations from the main configuration of the $1\ ^3A_2$ ground state. [d] Spin–orbit coupling constants.

Table 10 Selected electronic excited states of **12**.

State	Main configurations ($\|C\| > 0.3$)[a] C[b]	Character[c]	ΔE_{MRMP2}/cm^{-1}	SOCC[d]/cm^{-1}	D^{SO}_{zz}/cm^{-1}
$2\ ^1A_1$	−0.82	$14b_2 \rightarrow 9b_1$ (SOMO → SOMO)	22 591	35.71	0.0564
	−0.36	$9b_1 \rightarrow 14b_2$ (SOMO → SOMO)			
$3\ ^1A_1$	−0.93	$13b_2 \rightarrow 9b_1$ (lone pair → SOMO)	38 315	313.33	2.5623
$2\ ^3A_1$	−0.93	$13b_2 \rightarrow 9b_1$ (lone pair → SOMO)	38 365	318.82	−2.6495
$4\ ^1A_1$	0.77	$8b_1 \rightarrow 14b_2$ (π → SOMO)	44 921	41.00	0.0374
	−0.35	$7b_1 \rightarrow 14b_2$ (π → SOMO)			
$4\ ^3A_1$	0.71	$14b_2 \rightarrow 10b_1$ (SOMO → π*)	49 336	24.76	−0.0124
$1\ ^5A_1$	0.91	$13b_2 \rightarrow 10b_1$ (lone pair → π*)	59 383	188.16	0.1987
$8\ ^3A_1$	−0.80	$13b_2 \rightarrow 10b_1$ (lone pair → π*)	59 565	112.34	−0.2119
$9\ ^3A_1$	0.82	$13b_2 \rightarrow 10b_1$ (lone pair → π*)	65 514	77.09	−0.0907
$9\ ^1A_1$	0.87	$13b_2 \rightarrow 10b_1$ (lone pair → π*)	65 606	75.41	0.0867

[a] The active space consists of 10 orbitals: $3a_2$–$4a_2$, $6b_1$–$11b_1$, and $13b_2$–$14b_2$. [b] CAS-CI coefficients. [c] Excitation configurations from the main configuration of the $1\ ^3A_2$ ground state. [d] Spin–orbit coupling constants.